Backface Distance Fields: Relaxing Signed Distance Fields

Róbert Bán[a], Csaba Bálint[b] and Gábor Valasek[c]
Eötvös Loránd University, Faculty of Informatics, Department of Algorithms and their Applications, Hungary
{*rob.ban, csabix, valasek*}*@inf.elte.hu*

Keywords: Sphere Tracing, Signed Distance Fields, Ray-Surface Intersection, Unbounding Spheres, Safety Volumes.

Abstract: We propose backface distance functions, an implicit volume representation that improves the convergence rate of sphere tracing. We employ the closest signed distances to backfacing surface points, introducing a relaxed representation of signed distance functions. The backface and signed distance functions coincide within the volume. For external points, we prove that a backface distance-sized step is the largest direction-independent step along a ray that does not pass through the volume boundary more than once. We show analytic and discrete realizations of our concept. We present a discrete backface distance field generation method to construct exact and approximate fields from triangular meshes and procedural implicit scenes. We employ generation-time processing and correction steps in the discrete case to ensure robust surface visualization in combination with GPU filtering. We validate the proposed discrete and analytic representations empirically as well by comparing their performance to basic, relaxed, and enhanced sphere tracing and demonstrate that it generally outperforms the other methods.

1 INTRODUCTION

Signed distance functions (SDFs) and discrete signed distance fields provide versatile means to express and manipulate shapes of high geometric and topological complexity. Moreover, there are efficient means to directly render SDFs. The most popular iterative algorithm for the latter is Hart's sphere tracing (Hart, 1996) that operates on both analytic and discrete signed distance representations. Several variations have been proposed that improve its performance while preserving its robustness (Keinert et al., 2014; Bálint and Valasek, 2018). These approaches increase the trace step sizes based on user-provided hyper-parameters. Their optimal values depend on the scene and whether the input is analytic or discrete.

Our goal is to incorporate a relaxation into the signed distance representation itself that increases step sizes during intersection computations. In essence, we aim to find the SDF analogue of relaxed cone maps (Policarpo and Oliveira, 2007).

As such, we investigate the problem of robust and efficient ray-surface intersection computation from a representational perspective. We deviate from traditional signed distance descriptions by incorporating an isotropic relaxation into the representation itself via using shortest signed distances to backfacing surface points. We refer to these constructs as *backface distance functions* (BDF) and *discrete backface distance fields*.

We show that open spheres with such radii ensure that any ray originating from their center may only intersect the volume boundaries at most once. Moreover, these semidiameters are optimal sphere trace step sizes if ray directions are not known a priori. The BDF coincides with the SDF on the interior of volumes, allowing the sphere trace algorithm to render discrete and analytic BDFs.

Our main results are summarized as follows:

- We give a geometric and analytic characterization of backface distance functions and show that these are complete yet discontinuous volume representations.
- We derive the analytic BDF for several primitives and show empirically that these can be traced more efficiently than their SDF counterparts.
- We propose a discrete backface distance field representation that interpolates correctly with GPU trilinear filtering. It has the same storage requirements as a discrete SDF.
- We present a backface distance field generation algorithm that converts signed distance fields,

[a] https://orcid.org/0000-0002-8266-7444
[b] https://orcid.org/0000-0002-5609-6449
[c] https://orcid.org/0000-0002-0007-8647

Bán, R., Bálint, C. and Valasek, G.
Backface Distance Fields: Relaxing Signed Distance Fields.
DOI: 10.5220/0013251700003912

In *Proceedings of the 20th International Joint Conference on Computer Vision, Imaging and Computer Graphics Theory and Applications (VISIGRAPP 2025) - Volume 1: GRAPP, HUCAPP and IVAPP*, pages 127-138
ISBN: 978-989-758-728-3; ISSN: 2184-4321

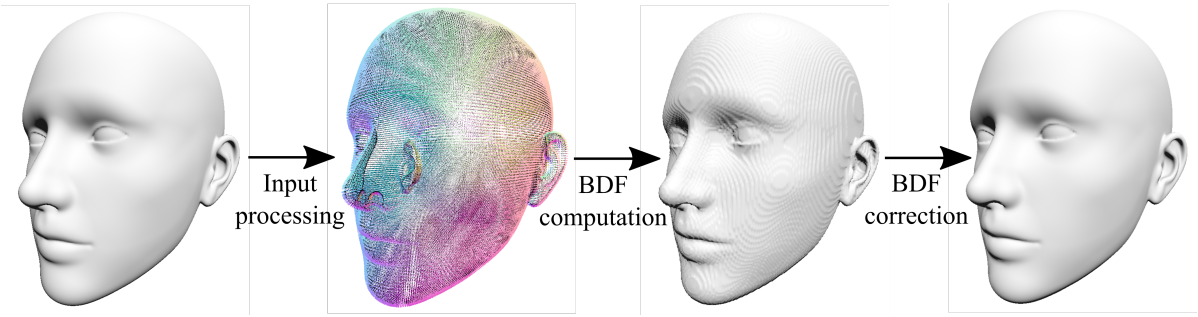

Figure 1: The three stages of our proposed backface distance field (BDF) generation process. First, an input-type dependent pre-processing step generates data to acquire surface boundary samples throughout the generation process. These samples may be actual geometric point-normal pairs from the surfaces or auxiliary data that accelerate surface traversals during BDF computations, such as initial parameter values for closest points for parametric boundaries. The second stage populates a 3D grid of samples with BDF values in accordance with Algorithm 1. Finally, a correction step, in Algorithm 2, takes this discrete BDF and expands the SDF region around the zero level set to preserve the original contour and, optionally, surface normals too. The 256^3 output BDF of the second stage is rendered at 0.48ms on an Nvidia 2080 GPU at 1920×1080 resolution, while the final silhouette- and normal-corrected BDF is rendered at 0.77ms. In comparison, the 256^3 SDF of the scene is rendered in 1.02ms on the same configuration.

signed distance functions, general implicits, and triangular meshes to our proposed representation.

In the following, Section 2 provides an overview of related work. Our theoretical results are presented in Section 3, where we provide a geometric and analytic characterization of the BDF and show that it is an exact volume representation.

Equipped with these geometric insights, we derive a simple, GPU-friendly BDF generation algorithm in Section 4 that is used to convert a variety of representations into BDFs. We highlight how runtime filtering footprints must be incorporated into the construction algorithm to ensure robustness of runtime rendering.

Section 5 presents how ray-surface intersections are computed on BDFs. In Section 6, we compare our method to various sphere tracing variants on analytic and discrete scenes. Finally, we discuss the advantages and limitations of our technique in Section 7 and conclude our paper.

2 RELATED WORK

2.1 Heightmap Rendering

Our research mainly aimed to identify the SDF equivalent of relaxed cone maps, a data structure used in heightfield rendering. Heightmaps augment coarser geometries with mesostructural detail. A wide range of algorithms have been proposed to compute the per-pixel exact or approximate ray-heightfield intersection (Szirmay-Kalos and Umenhoffer, 2008).

To find intersections, Dummer proposed to store the widest upward cone that does not overlap with the interior of the heightfield (Dummer, 2006). Their cone step mapping method intersects the rays with these cones to tend to the exact ray-heightfield intersection without skipping intersections.

A relaxation by expanding the cone angles was proposed in (Policarpo and Oliveira, 2007). The cones in this representation are the widest that allow a single intersection between a ray and the heightfield if the former is entering the heightfield volume from above. In contrast to conservative cones, relaxed cone maps guide the rays into the heightfield volume, thus they require a root refinement method, such as regula falsi, to find the precise ray-surface intersection. Depending on the step counts, relaxed cone step mapping provides a 5-20% performance improvement over conservative cone maps.

In terms of robustness, it must be noted that relaxed cone maps may skip over intersections for rays that are already within the heightfield volume. This issue was investigated in detail by Baboud et al. in (Baboud et al., 2012) and they resolved it by proposing an alternative representation that stores pre-computed safety distances. They also showed the importance of distances from backfacing triangles in the computation of the safety distances. More recently, it was shown in (Bán et al., 2024) that neither conservative nor relaxed cone maps interpolate correctly under bilinear interpolation, highlighting the importance of taking into account runtime filtering during cone map generation.

We set out to derive the SDF analogue to relaxed cone maps (Policarpo and Oliveira, 2007). We provide an exact geometric and analytic characterization of such constructs. We show both analytic and discrete realizations of our proposed representation and

verify that similar performance gains can be obtained to that of relaxed cone maps.

2.2 Signed Distance Representation

Signed distance functions are compact and expressive means to represent and visualize a wide range of shapes and their various combinations. These are used in various application domains, from physics, through geometric modeling, to computer graphics (Ohtake et al., 2001; Green, 2007; Wright, 2015; Evans, 2015; Angles et al., 2017; Osher and Fedkiw, 2003; Fuhrmann et al., 2003). As SDFs form a subset of implicit functions, they inherit the property that unions, intersections, and complements are expressed as maximum, minimum, and negation operations on the arguments (Bajaj et al., 1997). However, the resulting functions are generally signed distance lower bounds, not exact signed distances (Hart, 1996), although alternate set theoretic operation formulations have been proposed to preserve the distance property (Akleman and Chen, 2003).

It was noted (Hart, 1996; Kalra and Barr, 1989) that an SDF value paired with the point of evaluation defines an *unbounding sphere*, an open spherical volume that does not intersect with the boundaries of the scene. These are used to traverse a ray at variable step sizes without skipping over ray-surface intersections.

Keinert et al. (Keinert et al., 2014) proposed a step-size over-relaxation-based method to speed up sphere tracing. They use an $\omega \in [1,2)$ constant step size multiplier during trace and fall back to a traditional sphere trace step if the next guess produces an unbounding sphere that is disjoint from the previous.

Bálint et al. (Bálint and Valasek, 2018) reuse data from the current and previous steps to construct a linear approximation to the SDF function along the ray and use it to infer the closest ray parameter where the unbounding sphere is tangent to the current one. This is an optimal step size if the approximated surface is planar. Similarly to the over-relaxation method above, a basic sphere trace step is taken if the unbounding sphere is disjoint from the current one.

Galin et al. (Galin et al., 2020) proposed to compute local Lipschitz bounds along the ray, showing that it could provide more efficient rendering for a particular family of implicit functions. Their segment tracing technique offers high accuracy and does not require a fallback to sphere tracing, as all steps are safe. However, it does not apply to discrete representations, it is currently restricted to a subset of implicit representations, and even though it solves ray-surface intersection queries in a handful of steps, these iterations are costly computationally. Aydinlilar and Zanni (Aydinlilar and Zanni, 2023) propose to use bounds on the derivatives to infer conservative upper and lower bounds on the function value along the ray.

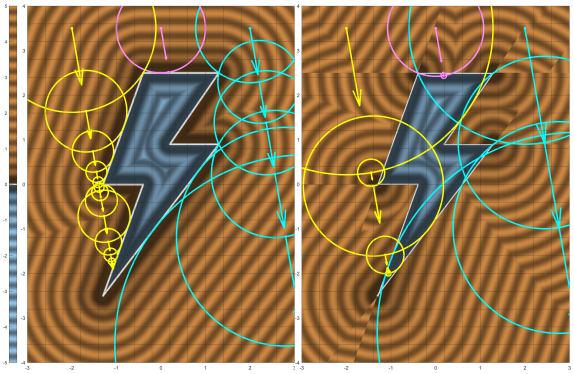

Figure 2: Signed distance function (left) and backface distance function (right) comparison in two dimensions. Three parallel rays are traced for each representation comparing how sphere tracing finds the closest intersection.

Our proposed representation has both analytic and discrete realizations. It is rendered by basic sphere tracing and does not require a hyperparameter. Moreover, we show that it outperforms basic, relaxed, and enhanced sphere tracing both for analytic and discrete input. As our representation coincides with SDFs in volume interiors, it trivially retains the same contour as SDFs, however, this requires a BDF correction step for the discrete case that we show in Section 4. BDFs are closed under union using the same functional point-wise minimum representation. Unlike SDF lower bounds, however, it is not closed under intersections and complements.

3 BACKFACE DISTANCE FUNCTIONS

In this section, we investigate the theoretical properties of backface distance functions. We present a geometric and analytic characterization of the boundary entities that function as the closest surface points for the BDF distance values. We also show that the BDF is an exact representation of the volume from which it was generated; as such, it is not merely an auxiliary acceleration structure for rendering but a complete volume representation.

3.1 Notation and SDFs

Let $\widehat{\boldsymbol{x}} = \frac{\boldsymbol{x}}{\|\boldsymbol{x}\|}$ denote the direction of $\boldsymbol{x} \neq \boldsymbol{0}$. The $c \in \mathbb{R}$ level set of an implicit function $f : \mathbb{R}^3 \to \mathbb{R}$ is written as $\{f = c\} = \{\boldsymbol{x} \in \mathbb{R}^3 \mid f(\boldsymbol{x}) = c\}$. Similarly, $\{f \leq c\} = \{\boldsymbol{x} \in \mathbb{R}^3 \mid f(\boldsymbol{x}) \leq c\}$. An $f : \mathbb{R}^3 \to \mathbb{R}$ function

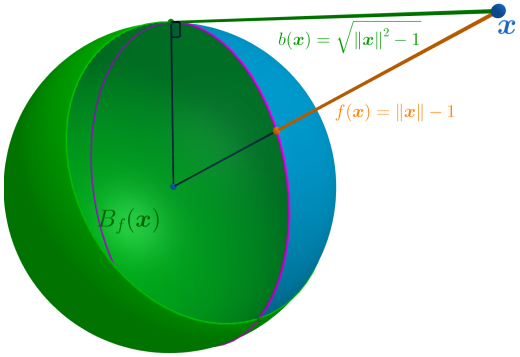

Figure 3: The length of the green line represents the value of the backface distance function of the unit sphere at point $\boldsymbol{x}$, whereas that of the orange segment represents the signed distance value. The green surface section is the backface surface set $B_f(\boldsymbol{x})$.

is a *distance function* (DF) if

$$f(\boldsymbol{x}) = d(\boldsymbol{x}, \{f = 0\}) \; = \inf\{\|\boldsymbol{x} - \boldsymbol{y}\| \;\mid\; f(\boldsymbol{y}) = 0\}, \tag{1}$$

and a *signed distance function* (SDF) if it is continuous and $|f|$ is a distance function (Bálint et al., 2019; Luo et al., 2019). Usually, we require the SDF to change sign when crossing the $\{f = 0\}$ surface for set operations and normal vector computation. The term *unbounding sphere* refers to the $|f(\boldsymbol{x})|$ radius open ball around $\boldsymbol{x} \in \mathbb{R}^3$, i.e. $k_{f(\boldsymbol{x})}(\boldsymbol{x}) = \{\boldsymbol{y} \in \mathbb{R}^3 \;\mid\; \|\boldsymbol{y} - \boldsymbol{x}\| < |f(\boldsymbol{x})|\}$, where f is an SDF.

3.2 BDF Definition and Geometry

Let us investigate the problem of finding the maximal open sphere such that any ray originating from its center intersects the volume boundaries within the sphere at most once. Generally, the radius of such a sphere may be formulated as the signed distance to the closest backface, i.e., points where the gradient points away from the center of the sphere. Formally, this is written as follows.

Definition 1. Assume that the $f : \mathbb{R}^3 \to \mathbb{R}$ SDF is differentiable on the $\{f = 0\}$ surface. The *backface surface* set $B_f(\boldsymbol{x})$ is defined for all $\boldsymbol{x} \in \mathbb{R}^3$ as

$$B_f(\boldsymbol{x}) = \{\boldsymbol{y} \in \{f = 0\} \;\mid\; \nabla f(\boldsymbol{y})^{\mathsf{T}} \cdot (\boldsymbol{y} - \boldsymbol{x}) \geq 0\}. \tag{2}$$

Definition 2. Assume that the $f : \mathbb{R}^3 \to \mathbb{R}$ SDF is differentiable on the $\{f = 0\}$ surface. The $b : \mathbb{R}^3 \to \mathbb{R}$ function is a *backface distance function* (BDF) if

$$b(\boldsymbol{x}) = \operatorname{sgn}(f(\boldsymbol{x})) \cdot d(\boldsymbol{x}, B_f(\boldsymbol{x})). \tag{3}$$

Note that this implies that the BDF coincides with the SDF inside the geometry, that is, for all $\boldsymbol{x} \in \{f \leq 0\} : b(\boldsymbol{x}) = f(\boldsymbol{x})$ holds. Moreover, since $B_f(\boldsymbol{x}) \subseteq \{f = 0\}$ for all $\boldsymbol{x} \in \mathbb{R}^3$, the backface distances are never less than the distance function, meaning $\big|f(\boldsymbol{x})\big| \leq \big|b(\boldsymbol{x})\big|$. This implies that the zero level-set is the same, so storing both functions is unnecessary solely for surface reconstruction. For example, the BDF of a sphere in Fig. 3 is

$$b_{sphere}(\boldsymbol{x}) = \begin{cases} \sqrt{\|\boldsymbol{x}\|^2 - 1} & \text{if } \|\boldsymbol{x}\| > 1 \\ \|\boldsymbol{x}\| - 1 & \text{if } \|\boldsymbol{x}\| \leq 1 \end{cases} \qquad \boldsymbol{x} \in \mathbb{R}^3 \tag{4}$$

For polygons and polyhedrons, we calculate it as the minimum distance to the backfacing sides. Figure 2 compares the exact SDF with the BDF.

Note that the BDF is not continuous. For example, each plane of any small planar surface patch separates the BDF into discontinuous partitions.

Let us now consider the problem of intersecting rays with backface distance functions. We show that taking a $|b(\boldsymbol{x})| - \varepsilon$ sized step in any direction from $\boldsymbol{x}$ may step over at most one root. If the sign of the function changed after a step, a single root was overstepped; and if the sign did not change, no surface intersection was skipped.

Proposition 1. Assume that the $\{b = 0\}$ surface is differentiable, where $b : \mathbb{R}^3 \to \mathbb{R}$ is its BDF. Then, for any $\boldsymbol{x} + t\widehat{\boldsymbol{v}}$ ray, the following equation has at most a single root in $t \in [0, b(\boldsymbol{x}) - \varepsilon]$ for any $\varepsilon > 0$:

$$b(\boldsymbol{x} + t\widehat{\boldsymbol{v}}) = 0 \tag{5}$$

Proof. We can assume that $\boldsymbol{x}$ is outside, that is, $b(\boldsymbol{x}) > 0$. First, we show that the set of solutions is at most finite, and then we prove that it cannot have two different elements. If there were a countable or otherwise infinite number of solutions within that interval, there would be an accumulation point around t^*, and any neighborhood around it contains an infinite amount of solutions. Since f is continuous, $f(\boldsymbol{x} + t^*\widehat{\boldsymbol{v}}) = 0$. This means $\nabla f(\boldsymbol{x} + t^*\widehat{\boldsymbol{v}})$ exists, and since f is an SDF, $\|\nabla f(\boldsymbol{x} + t^*\widehat{\boldsymbol{v}})\| = 1$, and this gradient must be perpendicular to the root series around t^*. This means that $\boldsymbol{x} + t^*\widehat{\boldsymbol{v}} \in B_f(\boldsymbol{x})$, which contradicts $t^* \leq b(\boldsymbol{x}) - \varepsilon$.

Let us assume that there are two neighboring solutions, $t_1 \neq t_2$. Since f is continuous and its gradient is non-diminishing, f must change signs from positive to negative and back. The sign change is the same as the sign of $\nabla f(\boldsymbol{x} + t_i\widehat{\boldsymbol{v}})^{\mathsf{T}} \cdot \widehat{\boldsymbol{v}}, i \in \{1,2\}$. Since the signs differ, one is positive at t_j ($j \in \{1,2\}$) which would mean that $\boldsymbol{x} + t_j\widehat{\boldsymbol{v}} \in B_f(\boldsymbol{x})$. This is a contradiction. □

The following observation simplifies the BDF generation by restricting the minimum distance search to points either on the silhouette or where the surface normal points to the opposite direction to the query position.

Proposition 2. Assuming a differentiable surface, let

$$B_f^c(\boldsymbol{x}) = \{\boldsymbol{y} \in \{f = 0\} \;\mid\; \nabla f(\boldsymbol{y})^{\mathsf{T}} \cdot \widehat{(\boldsymbol{y} - \boldsymbol{x})} = c\}, \tag{6}$$

for any $c \in [-1,1]$. Then, the backface distance function is

$$b(\boldsymbol{x}) = d\left(\boldsymbol{x}, B_f^0(\boldsymbol{x}) \cup B_f^1(\boldsymbol{x})\right). \tag{7}$$

Proof. Definition 2 is a conditional minimization problem on the closed set $M = \{\boldsymbol{y} \in \{f = 0\} \mid \nabla f(\boldsymbol{y})^\mathsf{T} \cdot (\boldsymbol{y} - \boldsymbol{x}) \geq 0\}$. Thus, the minimum either lies on the boundary of M or inside. In the former case, $\partial M \cap \{f = 0\} = B_f^0(\boldsymbol{x})$. If we omit the condition, we have a standard closest point problem where we minimize $\|\boldsymbol{y} - \boldsymbol{x}\|$ for $\boldsymbol{x}$ given that $f(\boldsymbol{y}) = 0$. Applying the Lagrange multiplier method gives the following equation for the derivative for some $\lambda \in \mathbb{R}$ parameter

$$\nabla L(\boldsymbol{y}) = \widehat{(\boldsymbol{y} - \boldsymbol{x})} + \lambda \nabla f(\boldsymbol{y}) = 0\,.$$

This means that $\widehat{(\boldsymbol{y} - \boldsymbol{x})}$ and $\nabla f(\boldsymbol{y})$ are parallel at the minimum. Because $\boldsymbol{y} \in M$, and f is an SDF so $\|\nabla f(\boldsymbol{y})\| = 1$ where differentiable, thus $\nabla f(\boldsymbol{y})^\mathsf{T} \cdot \widehat{(\boldsymbol{y} - \boldsymbol{x})} = 1$ in this case. □

Although the BDF is an SDF in the interior and on the boundary, it does not automatically inherit its ease of interoperability with set-theoretic operations. Let $b_1, b_2 : \mathbb{R}^3 \to \mathbb{R}$ be two BDFs. For union, we can take the pointwise minimum to bound the values from below via $\min(b_1, b_2) = \boldsymbol{x} \mapsto \min(b_1(\boldsymbol{x}), b_2(\boldsymbol{x}))$ to obtain a BDF of the $\{b_1 \leq 0\} \cup \{b_2 \leq 0\}$ objects. However, similar results do not hold for intersection, complement, or subtraction. That is, the maximum of two BDFs and the negation of a BDF does not yield a bound on the BDF of the intersection and complement operations, even though the minimum as a union operation yields a correct BDF outside.

4 BACKFACE DISTANCE FIELDS

Let us now consider the problem of generating BDF values for a grid of samples. At runtime, these samples are filtered to approximate the BDF. We present a method that converts various representations to discrete backface distance fields. The algorithm itself is composed of three stages, as illustrated by Fig. 1: i) input processing, ii) raw backface distance grid generation, and iii) backface distance field correction.

Input processing is not necessary for all input types. It generates data that accelerates closest-point computations via initial points or geometric proxies.

The *BDF generation* stage outputs a dense 3D grid of backface distance values. In general, boundary traversal and determination of the backfacing property are input-type dependent. Alternatively, it may be carried out on the proxy outputs generated in the input processing step.

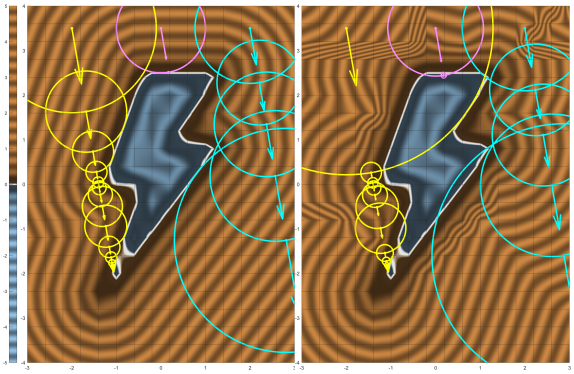

Figure 4: Interpolated SDF (left) and BDF (right) comparison in 2D. The surface and sphere tracing overstep due to interpolation have been fixed for the BDF.

In the *BDF correction* stage, the backface distances are further processed so that interpolation between samples yields a robustly traceable BDF approximation.

Since the BDF values can change discontinuously, the interpolated value of the stored exact samples can exceed the value of the true analytical BDF at the evaluation position. This can lead to distance overestimation while tracing the interpolated BDF, resulting in missing intersections. We solve this problem by modifying the stored BDF samples such that overstepping is prevented using the interpolated values.

We phrase these algorithms in terms of a general formalism that accommodates a wide variety of input geometry types. We introduce it next and apply it to the evaluation of the BDF.

4.1 Evaluating the BDF

The input geometry of the discrete BDF construction algorithm can be given by general implicit functions, analytic or discrete SDFs or lower bounds, parametric surfaces, or triangle meshes. To deal with all these cases in a concise manner, we introduce the following notational shorthands.

Let $V \subseteq \mathbb{R}^3$ denote a volume and $\partial V \subseteq \mathbb{R}^3$ its boundary. For any $\boldsymbol{p} \in \partial V$, let $\boldsymbol{n}(\boldsymbol{p})$ denote an unnormalized normal vector. Depending on the type of input geometry, it may be computed as, for example,

$$\boldsymbol{n}(\boldsymbol{p}) = \begin{cases} \nabla f(\boldsymbol{p}) & \text{for an implicit surface} \\ \partial_u \boldsymbol{r}(u,v) \times \partial_v \boldsymbol{r}(u,v) & \text{for a parametric surface} \\ (\boldsymbol{b} - \boldsymbol{a}) \times (\boldsymbol{c} - \boldsymbol{a}) & \text{for an } \boldsymbol{a},\boldsymbol{b},\boldsymbol{c}\text{triangle} \end{cases} \tag{8}$$

The evaluation of the BDF at an $\boldsymbol{x} \in \mathbb{R}^3$ point is the solution to

$$\min\left\{\|\boldsymbol{p} - \boldsymbol{x}\| \;\middle|\; \boldsymbol{p} \in \partial V, \boldsymbol{n}(\boldsymbol{p})^\mathsf{T} \cdot (\boldsymbol{p} - \boldsymbol{x}) \geq 0\right\} \tag{9}$$

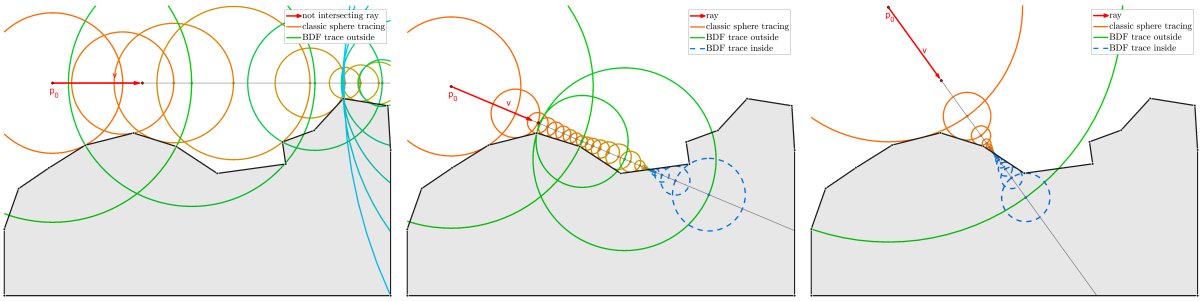

Figure 5: Three cases of tracing the SDF (in red) and the BDF (in green and blue) are displayed. On the left, the ray diverges to infinity, and our method leaves the frame in half as many steps. On the middle and the right, the ray intersects the surface, the BDF tracing steps inside and performs sphere tracing backwards to the root, rarely taking more steps (right).

with the sign $(-1)^{\chi_V(\boldsymbol{x})}$, where $\chi_V(\boldsymbol{x})$ is the characteristic function of V, i.e. $\chi_V(\boldsymbol{x}) = 1$ $(\boldsymbol{x} \in V)$ and $\chi_V(\boldsymbol{x}) = 0$ $(\boldsymbol{x} \notin V)$.

4.2 Input Processing

The input processing stage augments the input geometry with data that can be used to accelerate closest point queries.

For *implicit and SDF input*, our implementation generates surface point-normal pairs in this stage, and these samples replace the input function. This abstracts away the input for the next stage at the expense of precision. These pairs are stored in a linear buffer.

For *triangular meshes*, we skip this phase and compute the exact BDF value at each sample position. However, additional closest point query acceleration data may be built here, such as bounding volumes or space partitioning structures.

For *parametric boundaries*, this stage can generate a 3D grid where each sample stores a parametric patch identifier and the (u,v) parameters of the closest surface point to the sample position. Similarly, for implicit input, the closest boundary points may be stored. These can be used as initial guesses in the next stage of the algorithm when looking for the closest analytic backfaces.

4.3 BDF Grid Computation

Let $G \subseteq \mathbb{R}^3$ denote the set of discrete field sample positions defined on a grid. For example, in a grid with corner $\boldsymbol{g}_0 \in \mathbb{R}^3$, sample spacing $\Delta_x, \Delta_y, \Delta_z$, and resolution $(I+1) \times (J+1) \times (K+1)$, the grid positions are

$$G = \{\boldsymbol{g}_0 + (i\Delta_x, j\Delta_y, k\Delta_z) \mid i = 0..I, j = 0..J, k = 0..K\}. \quad (10)$$

Let $f[\boldsymbol{x}]$ and $b[\boldsymbol{x}]$ denote sample access for discrete signed and backface distance fields, respectively, where $\boldsymbol{x} \in G$ is a valid sample position. Our implementation indexes with (i,j,k) from Eq. (10).

Algorithm 1 is an input-agnostic pseudocode for generating discrete backface distance fields. The algorithm calculates the BDF value at each sample position $\boldsymbol{x} \in G$.

Inside the object, where $f[\boldsymbol{x}] \leq 0$, the BDF and SDF values coincide due to Definition 2. Outside the object, we iterate over all surface primitives and find the closest backfacing part. In practice, we compute the minimum of the squared distances and only apply the square root once at the end.

For implicit input, the primitives are surface samples in the form of $(\boldsymbol{p}, \widehat{\boldsymbol{n}})$ position-normal pairs from which the distance is $\|\boldsymbol{x} - \boldsymbol{p}\|$. A better distance approximation may be achieved with a closest point search starting from this sample (Saye, 2014). The surface sample is backfacing if the normal vector points away from the grid position: $(\boldsymbol{p} - \boldsymbol{x})^\mathsf{T} \cdot \widehat{\boldsymbol{n}} \geq 0$. We do not necessarily need a discrete SDF to determine the sign; the original implicit function can be used instead. If the signed distances are not known prior to BDF generation, we can calculate the SDF values alongside the BDF from the same surface samples.

4.3.1 Mesh Input

For mesh inputs, the triangle distances (Quilez, 2014) are calculated with Algorithm 4. Face orientation is determined according to Eq. (8). When a watertight mesh is supplied without its SDF, we calculate it alongside the BDF. Robust methods exist for sign determination (Baerentzen and Aanaes, 2005), yet ray casting worked well enough for our test cases.

The interpolation problem is partially solved within this step. During the generation of positive BDF values, the backfacing condition is relaxed to ensure that the interpolation is a lower bound where the exact BDF has discontinuities. To ensure the correctness of IsBackFacingPrimitive$(\boldsymbol{x}, s)$, we have to check whether the primitive is backfacing from any point within the cell of $\boldsymbol{x}$. The neighborhood that a

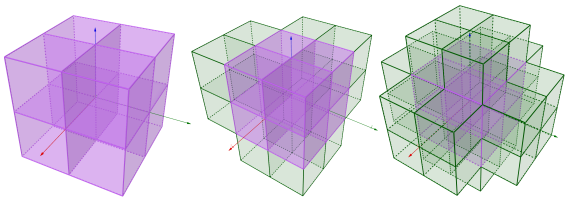

Figure 6: Closest neighbor search kernels for fixing the surface smoothness only (left), for normal calculation with the forward difference (middle), and for correct normal calculation with symmetric difference method (right).

grid sample influences during interpolation is

$$[\boldsymbol{x}_x-\Delta_x,\boldsymbol{x}_x+\Delta_x]\times[\boldsymbol{x}_y-\Delta_y,\boldsymbol{x}_y+\Delta_y]\times[\boldsymbol{x}_z-\Delta_z,\boldsymbol{x}_z+\Delta_z]. \quad (11)$$

The backfacing condition for the box is simplified to checking the farthest cell corner from the plane of the normal:

$$c=\boldsymbol{x}-(\mathrm{sgn}(\widehat{\boldsymbol{n}}_x)\Delta_x,\mathrm{sgn}(\widehat{\boldsymbol{n}}_y)\Delta_y,\mathrm{sgn}(\widehat{\boldsymbol{n}}_z)\Delta_z). \quad (12)$$

Then $\mathrm{IsBackFacingPrimitive}(\boldsymbol{x},s)=(\boldsymbol{p}-\boldsymbol{c})^{\mathsf{T}}\cdot\widehat{\boldsymbol{n}}\geq 0$.

Our BDF generation is implemented in compute shaders that execute in parallel for each sample on the GPU. Depending on the input size, the BDF generation is subdivided into several batches for better computing efficiency. If needed, the consecutive batches store the intermediate squared minimum distances.

Data: $G\subseteq\mathbb{R}^3$ set of grid positions, $f:G\to\mathbb{R}$ SDF, S set of surface primitives
Result: $b:G\to\mathbb{R}$ backface distance field
forall $\boldsymbol{x}\in G$ *sample position* **do**
  if $f[\boldsymbol{x}]\leq 0$ **then**
    $b[\boldsymbol{x}]\leftarrow f[\boldsymbol{x}]$;
  else
    $b[\boldsymbol{x}]\leftarrow+\infty$;
    forall $s\in S$ *surface primitive* **do**
      if *IsBackFacingPrimitive*$(\boldsymbol{x},s)$ **then**
        $d\leftarrow\mathrm{DistanceToPrimitive}(\boldsymbol{x},s)$;
        $b[\boldsymbol{x}]\leftarrow\min(b[\boldsymbol{x}],d)$;
      end
    end
  end
end

Algorithm 1: Calculating discrete BDFs (stage 2).

4.4 BDF Correction

The final stage of discrete BDF generation ensures correct interpolation near the surface. As the true analytical BDF can have discontinuities or singularities along the surface, the interpolated surface will be offset and exhibit wrinkles and artifacts along cell boundaries. The surface is corrected by replacing the stored larger BDF values with SDF values near the surface. In Algorithm 2, we replace the stored values if any of its neighbors are negative. The shapes and sizes of this neighborhood kernel are visualized in Fig. 6. When high-quality surface normals are not required, we may correct within the smallest neighborhood to retain more performance of the BDF. Surface normal calculations rely on numeric differentials that may become faulty on cell boundaries when the next cell contains much larger BDF values. We have to use a larger search kernel for the correct symmetric and one-sided differentials.

Data: $G\subseteq\mathbb{R}^3$ set of grid positions, $f:G\to\mathbb{R}$ SDF, $b:G\to\mathbb{R}$ backface distance field
Result: $b:G\to\mathbb{R}$ modified BDF
forall $\boldsymbol{x}\in G$ *sample position* **do**
  forall $\boldsymbol{y}\in$ *NeighbourSamples*$(\boldsymbol{x})$ **do**
    if $f[\boldsymbol{y}]\leq 0$ **then**
      $b[\boldsymbol{x}]\leftarrow f[\boldsymbol{x}]$;
      break;
    end
  end
end

Algorithm 2: Correcting discrete BDFs (stage 3).

5 RENDERING BACKFACE REPRESENTATIONS

The common advantage of analytic and discrete backface distance representations is the simplicity of the rendering algorithm: the sphere tracing algorithm, listed in Algorithm 3. Since a BDF-sized step may leap into the volume, the trace then starts going backward via negative stepsizes in a basic sphere tracing fashion as in Fig. 5.

Data: $\boldsymbol{p}_0+t\widehat{\boldsymbol{v}}$ ray, $\boldsymbol{b}:\mathbb{R}^3\to\mathbb{R}$ BDF
Result: $t\geq 0$ distance traveled to the first intersection
$t\leftarrow 0$; $i\leftarrow 0$;
repeat
  $r\leftarrow b(\boldsymbol{p}_0+t\widehat{\boldsymbol{v}})$;
  $t\leftarrow t+r$;
  $i\leftarrow i+1$;
until $|r|<\varepsilon$ ***or*** $t\geq t_{\max}$ ***or*** $i\geq i_{\max}$;

Algorithm 3: Sphere tracing a BDF.

Due to the interpolation error in the discrete case, the sphere trace on the inferred SDF might step outside once again; however, the interpolation error is smaller than the cell size. This means that the corrected BDF in that cell equals the SDF and will converge to the trilinear surface. While sphere tracing using SDFs finds the solution without ever allowing the tracing to enter the volume, tracing with BDFs often guides the steps inside the volume and simultaneously flips the tracing direction. Sphere tracing of the two

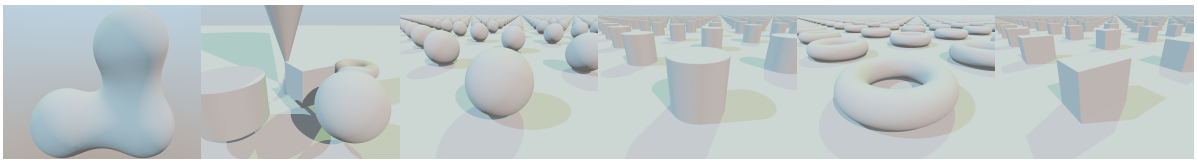

Figure 7: Procedural scenes used in our analytic BDF performance tests, including blobs and various primitives.

representations is compared in Fig. 2 for the analytic case and in Fig. 4 for a 2D discrete BDF field.

Experimental algorithms that explicitly split the loop into two phases, one for exterior and one for internal trace, proved to be much slower. Even if we employ root-finding methods upon the first sign change, such as bisection or regula-falsi, the performance is lower than the sphere tracing algorithm above.

A slight modification to the tracing algorithm allows for faster shadow calculation. Since the BDF guarantees that a sphere tracing step only skips at most one intersection point, we can stop tracing at the first sign change. In practice, this means stopping when $r < \varepsilon$ instead of $|r| < \varepsilon$ in Algorithm 3.

6 TEST RESULTS

We tested our proposed analytic and discrete BDF representations in rendering scenarios, and compared performance statistics to basic (Hart, 1996), relaxed (Keinert et al., 2014), and enhanced sphere tracing (Bálint and Valasek, 2018), adapting the nomenclature from the latter. Algorithm 3 was used for BDF rendering. We manually selected a relaxation parameter $\omega = 1.6$ for relaxed sphere tracing and $\omega = 0.88$ for enhanced sphere tracing, providing the best speed-up while retaining geometric accuracy.

We implemented the tracing and generation methods in the NVIDIA Falcor (Kallweit et al., 2022) framework in C++ with DirectX 12 backend. We ran tests on triangular meshes and procedural scenes adapted from (Takikawa et al., 2022). Measurements were taken with both AMD and NVIDIA GPUs in a resolution of 1920×1080. The distance fields were stored in 16-bit half-precision 3D textures. The full implementation will be released.

6.1 BDF Correction

The samples in a discrete BDF differ from simple backface distance function evaluations, as shown in Section 4.3 and Section 4.4 These are necessary because a raw, unprocessed discrete BDF with runtime trilinear filtering results in blocky renders, such as shown in Fig. 1. However, these processing steps also affect real-time performance considerably.

For the bunny mesh, the processed field was 24% and 53% slower at 32 and 1000 iterations than the raw BDF, respectively. The same correction-induced performance loss ratios for the Möbius strip amounted to an average of 19% and 41% on Nvidia 2080 and 16% and 35% on AMD RX 5700.

6.2 Performance of Analytic BDFs

Table 1 summarizes our performance measurements on procedural scenes, shown in Fig. 7. The derivation and implementation of BDF functions are located in our Appendix.

Overall, BDF primitives offered minor to modest performance improvements over their SDF counterparts in 85% of our tests. Shadow rays traced the same type of procedural geometry as the primary traces. This made BDFs even more efficient in scenes involving shadows, as our representation guides rays into the volumes. A distinct exception was the Box scene which shows the need for a more efficient BDF approximation to the box primitive. On the other scenes, BDFs were 7% and 11% more performant on AMD and Nvidia than SDFs on average using shadows.

We compared the performance of BDF tracing to Lipschitz segment tracing (Galin et al., 2020) on a scene adapted from the authors' ShaderToy sample. On AMD RX 5700, Lipschitz segment tracing required 45% of the frame time of sphere tracing while our method only needed 38%. Lipschitz and BDF numbers on the Nvidia 2080 GPU are 48% and 40%, respectively, showing that BDF tracing outperforms Lipschitz segment tracing on SDF-like implicit functions.

6.3 Performance of Discrete BDFs

First, we measured the render time performance implications of different field sizes, ranging from 64^3 to 512^3. On the highest resolution, discrete BDFs are unequivocally more efficient (13-25% on average, in some cases up to 35%) than basic sphere tracing; however, the dilation of the SDF area to preserve contours and shading normals severely hinders them at smaller fields. Consequently, BDF gains are more

Table 1: Performance comparison of sphere tracing on procedural signed and backface distance functions (SDF and BDF columns) with and without hard shadows. Shadow rays are traced on the same representation as the primary rays. Timings on the SDFs are reported in milliseconds, BDF numbers are relative to sphere tracing, and the resolution was 1920×1080.

		Box		**Cylinder**		**Primitives**		**Sphere**		**Torus**	
GPU	**Shadow**	**SDF**	**BDF**	**SDF**	**BDF**	**SDF**	**BDF**	**SDF**	**BDF**	**SDF**	**BDF**
AMD RX 5700	**ON**	1.517	135%	1.66	99%	3.155	96%	1.285	83%	1.614	93%
	OFF	0.683	142%	0.72	110%	1.345	101%	0.555	91%	0.694	96%
NVIDIA 2080	**ON**	0.93	133%	1.15	83%	1.66	88%	1.07	87%	1.62	97%
	OFF	0.4	130%	0.53	96%	0.75	89%	0.38	87%	0.47	81%

Table 2: Frame render times for NVIDIA 2080 Super for three procedural and two triangular mesh scenes with or without shadows for sphere tracing (ST), relaxed sphere trace (RT) (Keinert et al., 2014), enhanced sphere tracing (ET) (Bálint and Valasek, 2018), and our BDF sphere trace method. Sphere tracing runtimes are in milliseconds, the others are relative to those.

		Shadows: off				Shadows: on			
Scene	Steps	ST	RT	ET	BDF	ST	RT	ET	BDF
Spheres	32	0.43	105%	109%	**86%**	0.66	105%	114%	**85%**
	1000	0.77	92%	93%	**77%**	1.14	87%	89%	**75%**
Gears	32	0.28	104%	104%	**89%**	0.39	103%	105%	**87%**
	1000	0.37	92%	89%	**86%**	0.5	90%	90%	**84%**
Mountain	32	0.36	100%	106%	**78%**	0.55	93%	104%	**75%**
	1000	0.49	86%	96%	**71%**	0.67	84%	96%	**72%**
Bunny mesh	32	0.25	100%	100%	**88%**	0.33	101%	102%	**86%**
	1000	0.32	92%	**86%**	**86%**	0.39	92%	90%	**85%**
Skull mesh	32	0.23	104%	104%	**91%**	0.31	106%	106%	**90%**
	1000	0.45	84%	**82%**	89%	0.51	**88%**	94%	90%

modest (7-11%) at the smallest resolutions.

For the performance comparison between basic, enhanced, relaxed, and BDF sphere tracing, we choose the resolution of 128^3. We computed exact BDF fields for mesh inputs and approximate ones for procedural SDFs. BDF generation times at this resolution were between 0.5-80 seconds on both GPUs, depending on the input geometry. For meshes, SDF and BDF generation times were effectively identical. The measurements in Table 2 were taken at 1920×1080 resolution. We recorded timings at low (32) and high (1000) iteration limits.

BDFs performed significantly better on fields generated from procedural inputs (19% and 22% faster on average than sphere tracing with and without shadows on both AMD RX 5700 and Nvidia 2080 Super, respectively) compared to mesh inputs (9% and 12% faster with and without shadows on the AMD GPU, 12% for both on the Nvidia card). At high iteration counts, relaxed and enhanced sphere tracing approached or occasionally outperformed BDF traces, the latter occurring 3.125% of the times in our tests.

The tests showed that high-resolution fields mask the performance implications of dilating the SDF region within the discrete BDFs. This is explained by the smaller absolute volumes on which the SDF is reinstated. Even with our representation, the silhouettes are hotspots for iterations, but much less so.

However, note that performance also drops due to the more conservative backface selection property that takes into account the filtering footprint when selecting prospective backfaces. Further research is needed to identify if the gap between raw and corrected discrete BDFs can be narrowed by different processing at generation time or by other filtering techniques beyond trilinear at runtime.

7 CONCLUSIONS

We proposed a new volumetric representation, backface distance functions. These constructs compute the signed distances to the closest backfaces and efficiently resolve ray-surface intersections.

We investigated the mathematical properties of backface distance functions and proved that they provide a complete geometric description of the scene without any additional data. We presented procedural backface distance functions for various primitives and derived a discrete realization that takes filtering into account.

We proposed a three-stage algorithm to generate exact and approximate discrete backface distance fields from triangular mesh and procedural implicit inputs. The main contribution here is how we pre-

serve the same silhouette and shading normal as a discrete signed distance field via additional processing steps.

Our performance tests showed that tracing on our analytic and discrete representations is more efficient than various trace methods on signed distance functions and fields. Our representation is almost matched or slightly outperformed by the other algorithms at very high iteration count limits for a limited set of inputs. However, this also shows that the shape-preservation steps hinder the acceleration potential of backface distance fields. We verified this with measurements that up to 41% performance gain is lost compared to raw backface distance fields. Nevertheless, in general, tracing on our representation converges faster initially, requiring fewer iterations than the other methods.

Further research is required to mitigate the performance loss due to discrete backface distance field correction, either via generation-time processing or runtime filtering. Similarly, procedural backface distance function approximations to the results of intersection and complement set-theoretic operations are subject to future work.

REFERENCES

Akleman, E. and Chen, J. (2003). Constant Time Updateable Operations for Implicit Shape Modeling.

Angles, B., Tarini, M., Wyvill, B., Barthe, L., and Tagliasacchi, A. (2017). Sketch-based Implicit Blending. *ACM Transactions on Graphics*, 36(6):1–13.

Aydinlilar, M. and Zanni, C. (2023). Forward inclusion functions for ray-tracing implicit surfaces. *Computers & Graphics*, 114:190–200.

Baboud, L., Eisemann, E., and Seidel, H.-P. (2012). Precomputed Safety Shapes for Efficient and Accurate Height-Field Rendering. *IEEE Transactions on Visualization and Computer Graphics*, 18(11):1811–1823.

Baerentzen, J. and Aanaes, H. (2005). Signed Distance Computation Using the Angle Weighted Pseudonormal. *IEEE Transactions on Visualization and Computer Graphics*, 11(3):243–253.

Bajaj, C., Blinn, J., Cani, M.-P., Rockwood, A., Wyvill, B., and Wyvill, G. (1997). *Introduction to Implicit Surfaces*. Morgan Kaufmann Publishers Inc., San Francisco, CA, USA.

Bálint, C. and Valasek, G. (2018). Accelerating Sphere Tracing. In *EG 2018 - Short Papers*, page 4 pages, Delft, Netherlands. The Eurographics Association.

Bálint, C., Valasek, G., and Gergó, L. (2019). Operations on Signed Distance Functions. *Acta Cybernetica*, 24(1):17–28.

Bán, R., Valasek, G., Bálint, C., and Vad, V. A. (2024). Robust cone step mapping. In Haines, E. and Garces, E., editors, *Eurographics symposium on rendering*. The Eurographics Association. ISSN: 1727-3463.

Dummer, J. (2006). Cone Step Mapping: An Iterative Ray-Heightfield Intersection Algorithm.

Evans, A. (2015). Learning from Failure: a Survey of Promising, Unconventional and Mostly Abandoned Renderers for 'Dreams PS4', a Geometrically Dense, Painterly UGC Game. In *Advances in Real-Time Rendering in Games*. SIGGRAPH, MediaMolecule.

Fuhrmann, A., Sobotka, G., and Groß, C. (2003). Distance fields for rapid collision detection in physically based modeling. *International Conference Graphicon 2003*.

Galin, E., Guérin, E., Paris, A., and Peytavie, A. (2020). Segment Tracing Using Local Lipschitz Bounds. *Computer Graphics Forum*, 39(2):545–554.

Green, C. (2007). Improved Alpha-tested Magnification for Vector Textures and Special Effects. In *ACM SIGGRAPH 2007 courses on - SIGGRAPH '07*, SIGGRAPH '07, pages 9–18, San Diego, California. ACM Press.

Hart, J. C. (1996). Sphere Tracing: A Geometric Method for the Antialiased Ray Tracing of Implicit Surfaces. *The Visual Computer*, 12(10):527–545.

Kallweit, S., Clarberg, P., Kolb, C., Davidovič, T., Yao, K.-H., Foley, T., He, Y., Wu, L., Chen, L., Akenine-Möller, T., Wyman, C., Crassin, C., and Benty, N. (2022). The Falcor Rendering Framework.

Kalra, D. and Barr, A. H. (1989). Guaranteed Ray Intersections with Implicit Surfaces. In *16th Annual Conference on Computer Graphics and Interactive Techniques*, SIGGRAPH '89, pages 297–306, New York, NY, USA. Association for Computing Machinery.

Keinert, B., Schäfer, H., Korndörfer, J., Ganse, U., and Stamminger, M. (2014). Enhanced Sphere Tracing. In *Smart Tools and Apps for Graphics - Eurographics Italian Chapter Conference*, page 8 pages. The Eurographics Association.

Luo, H., Wang, X., and Lukens, B. (2019). Variational Analysis on the Signed Distance Functions. *Journal of Optimization Theory and Applications*, 180(3):751–774.

Ohtake, Y., Belyaev, A., and Pasko, A. (2001). Dynamic meshes for accurate polygonization of implicit surfaces with sharp features. In *International Conference on Shape Modeling and Applications*, pages 74–81, Genova, Italy. IEEE Computer Society.

Osher, S. and Fedkiw, R. (2003). Signed Distance Functions. In Antman, S. S., Marsden, J. E., and Sirovich, L., editors, *Level Set Methods and Dynamic Implicit Surfaces*, volume 153, pages 17–22. Springer New York, New York, NY. Series Title: Applied Mathematical Sciences.

Policarpo, F. and Oliveira, M. M. (2007). Relaxed Cone Stepping for Relief Mapping. In *GPU Gems 3*.

Quilez, I. (2014). Distance to a Triangle.

Saye, R. (2014). High-order methods for computing distances to implicitly defined surfaces. *Communications in Applied Mathematics and Computational Science*, 9(1):107–141.

Szirmay-Kalos, L. and Umenhoffer, T. (2008). Displacement Mapping on the GPU - State of the Art. *Computer Graphics Forum*, 27(6):1567–1592.

Takikawa, T., Glassner, A., and McGuire, M. (2022). A Dataset and Explorer for 3D Signed Distance Functions. *Journal of Computer Graphics Techniques (JCGT)*, 11(2):1–29.

Wright, D. (2015). Dynamic Occlusion with Signed Distance Fields. Epic Games (Unreal Engine).

APPENDIX

Analytic Backface Distance Functions

In this section, we list some of the analytic backface distance primitives along with their SDF counterparts when evaluating at an $\boldsymbol{x} = [x,y,z]^\mathsf{T}$ query point.

Unit Sphere

We have to calculate the length of a segment tangential to the sphere from the $\boldsymbol{x}$ query point.

SDF: $f(\boldsymbol{x}) = \|\boldsymbol{x}\| - 1$

BDF: $b(\boldsymbol{x}) = \begin{cases} \sqrt{\|\boldsymbol{x}\|^2 - 1} & \text{if } f(\boldsymbol{x}) > 0 \\ f(\boldsymbol{x}) & \text{if } f(\boldsymbol{x}) \leq 0 \end{cases}$

The difference between the BDF and the SDF for the sphere is

$$b_{sphere}(\boldsymbol{x}) - f_{sphere}(\boldsymbol{x}) = \sqrt{\|\boldsymbol{x}\|^2 - 1} - \|\boldsymbol{x}\| + 1,$$

where $\|\boldsymbol{x}\| > 1$. This difference approaches 1 as $\|\boldsymbol{x}\| \to \infty$. In practice, tracing a BDF takes larger steps by the sphere radius but slows down near the surface because of local concavity. However, the slowdown near the surface is much smaller because $\lim_{\|\boldsymbol{x}\|\to 0} \frac{b(\boldsymbol{x})}{f(\boldsymbol{x})} = +\infty$.

Infinite Cylinder

The equation for the cylinder is the same, except that it only needs two dimensions.

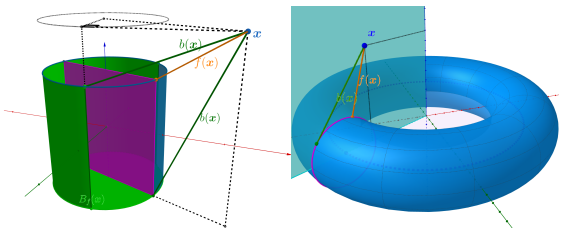

(a) Finite cylinder (b) Torus

Figure 8: Geometry of the BDF and its construction for the two primitives. The green surface on the finite cylinder is the backface surface set $B_f(\boldsymbol{x})$ as seen from query point $\boldsymbol{x}$.

SDF: $f(x,y,z) = \sqrt{x^2+y^2} - 1$

BDF: $b(x,y,z) = \begin{cases} \sqrt{x^2+y^2-1} & \text{if } f(x,y,z) > 0 \\ f(x,y,z) & \text{if } f(x,y,z) \leq 0 \end{cases}$

The formula for the finite cylinder is more involved. Figure 8a aids with interpreting the source code.

Infinite Cone

The cone is similar to the cylinder, the radius changes with the z coordinate. From now on, we always assume that $b(x,y,z) = f(x,y,z)$ when $f(x,y,z) < 0$, so we only list when $f(x,y,z) > 0$.

SDF: $f(x,y,z) = \frac{\sqrt{x^2+y^2} - z\tan\alpha}{1+\tan^2\alpha}$

BDF: $b(x,y,z) = \sqrt{x^2+y^2-(z\tan\alpha)^2}$

Torus

The BDF of the torus is visualized in Fig. 8b.

SDF: $f(x,y,z) = \sqrt{\left(\sqrt{x^2+y^2} - R\right)^2 + z^2} - r$

BDF: $b(x,y,z) = \left(\sqrt{x^2+y^2} - R\right)^2 + z^2 - r$

Data: $G \subseteq \mathbb{R}^3$ set of grid positions, and T set of triangles, $\boldsymbol{dir} = [1,0,0]^\mathsf{T}$ arbitrary direction for sign determination
Result: $f : G \to \mathbb{R}$ signed distance field, and $b : G \to \mathbb{R}$ backface distance field
forall $\boldsymbol{x} \in G$ *sample position* **do**
  $b2 \leftarrow +\infty$;
  $f2 \leftarrow +\infty$;
  $sign \leftarrow 1$;
  forall $t \in T$ *triangle* **do**
    $d2 \leftarrow$ SquaredDistanceToTriangle$(\boldsymbol{x}, t)$;
    $f2 \leftarrow \min(f2, d2)$;
    if *IntersectTriangle*$(\boldsymbol{x}, \boldsymbol{dir}, t)$ **then**
      $sign \leftarrow -sign$;
    end
    if *IsBackFacingTriangle*$(\boldsymbol{x}, t)$ **then**
      $b2 \leftarrow \min(b2, d2)$;
    end
  end
  $f[\boldsymbol{x}] \leftarrow sign \cdot \sqrt{f2}$;
  $b[\boldsymbol{x}] \leftarrow sign \cdot \sqrt{b2}$;
end

Algorithm 4: Calculating SDF and BDF for a mesh.

Plane

The BDF values of a plane with unit normal $\hat{\boldsymbol{n}} \in \mathbb{R}^3$ are infinite throughout the whole positive half-space because the surface has no backfaces viewed from there. We rectify this by setting an arbitrary value in

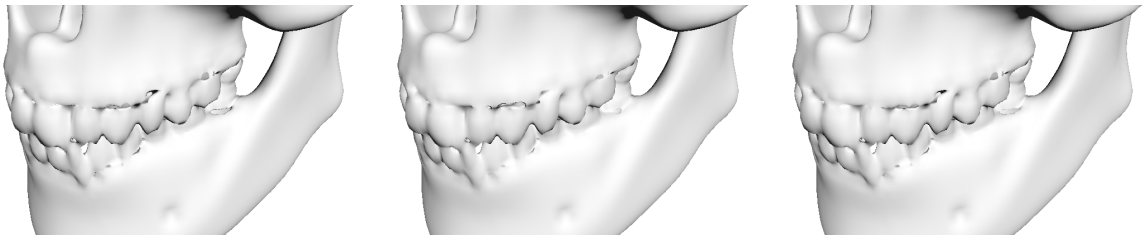

(a) SDF. (b) Non-conservative BDF. (c) Conservative BDF.

Figure 9: Comparison of baseline SDF (left) to post-processed but non-conservatively (center) and conservatively (right) generated 128^3 BDFs.

the following shader code to allow the sphere tracing to trace backward from there. Due to the sphere tracing slowdown near the surface, this change is actually much faster than the regular SDF plane, especially if the horizon is in view.

SDF: $f(\boldsymbol{x}) = \boldsymbol{x}^\mathsf{T} \cdot \widehat{\boldsymbol{n}}$

BDF: $b(\boldsymbol{x}) = \begin{cases} +\infty & \text{if } f(\boldsymbol{x}) > 0 \\ f(\boldsymbol{x}) & \text{if } f(\boldsymbol{x}) \leq 0 \end{cases}$

Data: $\boldsymbol{c} \in \mathbb{R}^3$ starting grid corner, $(I,J,K) \in \mathbb{N}^3$ grid resolution, $\Delta \in \mathbb{R}^+$ grid spacing, $f : \mathbb{R}^3 \to \mathbb{R}$ SDF, $\rho \in (0,1]$ search step relaxation
Result: $S \subseteq \mathbb{R}^3 \times \mathbb{R}^3$ set of position-normal pairs (surface samples)

```
S ← ∅;
forall p ∈ {c + Δ·[i,j,k]^T | 0 ≤ i < I, 0 ≤ j < J, 0 ≤ k < K} do
    if |f(p)| ≤ √3·Δ then
        q ← p; m = 0 ;
        while |f(q)| > ε ∧ m < m_max do
            q ← q − ρ·f(q)·∇f(q);
            m ← m + 1;
        end
        S ← S ∪ {(q, ∇f(q))};
    end
end
```

Algorithm 5: Surface sample generation from SDF.

General Construction Algorithm

Algorithm 4 calculates both the SDF and the BDF from a mesh, while Algorithms 5 and 6 generates BDF from SDF through surface samples. In practice, the visual difference is negligible between the SDF and the corrected BDF because both use the same tracing algorithm as demonstrated on Fig. 9.

BDF Tracing Variant

In practice, we often employ the robust variant of BDF sphere tracing seen in Algorithm 3. In addition to the usual termination condition, this method also terminates when the BDF changes sign during the backward sphere tracing. The advantage is that this method converges even if the BDF was not corrected. The BDF texture lookup completely hides the time it takes to evaluate the additional condition, thus the render times for the two variants were exactly equal.

Data: $G \subseteq \mathbb{R}^3$ set of grid positions, $f : G \to \mathbb{R}$ SDF, $S \subseteq \mathbb{R}^3 \times \mathbb{R}^3$ set of surface samples
Result: $b : G \to \mathbb{R}$ backface distance field

```
forall x ∈ G sample position do
    if f[x] ≤ 0 then
        b[x] ← f[x];
    else
        b2 ← +∞ ;
        forall (p, n) ∈ S position-normal pair do
            if IsBackFacingSample(x, p, n) then
                d2 ← ‖p − x‖^2 ;
                b2 ← min(b2, d2) ;
            end
        end
        b[x] ← √b2;
    end
end
```

Algorithm 6: Calculating BDF for an SDF.